

International Conference on Space Optics—ICSO 2022

Dubrovnik, Croatia

3–7 October 2022

Edited by Kyriaki Minoglou, Nikos Karafolas, and Bruno Cugny,



Verification of straylight rejection of optical science payloads using a pulsed laser source



Verification of straylight rejection of optical science payloads using a pulsed laser source

Antoine Ummel^{*a}, Jean-Christophe Roulet^{** a}, Jannis Holzer^a, Fabien Droz^a, Thomas Weigel^b,
Lionel Clermont^c, Marc Georges^c, Juliana Abrantes^d, Dana Tomuta^e, Kate Isaak^e, Dominc Doyle^e,
Micael Miranda^f, Christophe Pache^a,

^aCSEM, Centre Suisse d'Electronique et de Microtechnique, Rue Jaquet-Droz 1, 2000 Neuchâtel,
SWITZERLAND;

^bThales Alenia Space Switzerland, Schaffhauserstrasse 580, 8052 Zürich, SWITZERLAND;

^cCentre Spatial de Liège (CSL), STAR Institute, Université de Liège, Avenue du Pré-Aily , 4031
Angleur, BELGIUM;

^dLusospace, Rua Sarmiento Beires, 31A, 1900-411 Lisboa, PORTUGAL;

^eEuropean Space Agency ESTEC, Keplerlaan 1, 2201-AZ Noordwijk, THE NETHERLAND;

^fATG Europe BV, Huygensstraat 34, 2201 DK Noordwijk, THE NETHERLAND.

ABSTRACT

The performance of astronomical space telescopes can be greatly impacted by straylight. That is why characterizing the straylight in such telescopes before they are deployed is paramount. Nowadays such characterization can be done by simulation or by test. Simulation can provide very useful information on the origin of straylight, helping devise solutions to reduce it and improve the performance of the telescope. However, simulation suffers from limitations due to processing power needed and assumptions made in the model which can lead to simulation results quite far from the actual performances. Standard straylight tests on the other hand provide accurate measurement of the straylight but without any insight about its origin, making it difficult to mitigate.

Emerging technologies now offer new possibilities for straylight measurement using time-of-flight technics to help identify the origin of the straylight. Such technologies were reviewed and analysed in a first activity called TRIPP (Time-Resolved Imaging of Photon Paths). The results and outcome of this study are presented in the first chapter of this paper. A second chapter then presents the ongoing status of a second activity, SLOTT (Straylight Lidar Oqse verificaTion Tool) which aims to develop a demonstrator for such a time-resolved straylight verification system.

With the development and test of such a tool, CSEM and its partners (TAS-CH, Difrotec, CSL, LusoSpace), supported by ESA, hopes to establish new methods to characterize and reduce the straylight propagation in future space-based telescopes.

Keywords: Straylight, LiDAR, Time-of-Flight, Time-resolved, Telescope, Photon counting, CHEOPS

1. INTRODUCTION

For astronomical space telescopes, straylight represents a major issue and can seriously degrade image quality and performance. During the development of a telescope, being able to identify the origin of stray light is essential to implement mitigations and design improvements, thus reducing the straylight and improving the telescope performance.

While simulation tools can provide some information about the straylight path, they suffer from the typical limitations of most simulation tools: significant efforts are needed to perform the processing and the simulation results sometimes deviate from the measured performance due to assumptions made, consciously or unconsciously, in the model. On the other hand,

* antoine.ummel@csem.ch; phone: +41 32 720 59 12; csem.ch

** jean-christophe.roulet@csem.ch; phone: +41 32 720 59 41; csem.ch

state-of-the-art straylight measurement setups provide good measurements of the resulting telescope performance, but they provide very little to no information about the origin of the observed straylight.

The present paper describes how emerging technologies can enable the use of time-of-flight techniques to improve the capabilities of the next generation of straylight verification tools. Such a tool would also benefit from being transportable: it could then be used directly in payloads integration labs, limiting the need for dedicated test infrastructure.

The first chapter of this paper presents the results of TRIPP (Time-Resolved Imaging of Photon Paths), a feasibility study commissioned by ESA. This study aimed to assess the suitability of state-of-the-art time-of-flight technologies for straylight measurement.

The second chapter presents the current design of the breadboard developed in the frame of the project SLOTT (Straylight Lidar Oqse verificalTion Tool) development commissioned by ESA. This breadboard aims to validate the capabilities of such a system and will be tested onto a representative target: the CHEOPS Baffle STM.

2. TRIPP – HOW TIME-OF-FLIGHT TECHNIQUES CAN IMPROVE OUR UNDERSTANDING OF STRAYLIGHT IN A TELESCOPE

The TRIPP study was a project funded by an "express procurement" - EXPRO+ program from ESA, aiming to investigate solutions to perform time-resolved measurement of straylight path in space telescopes. Thus, the activity started with a review of the state-of-the-art time-resolved imaging technics which is described in section 2.1. Then, an analysis of the expected performance of such a system is discussed. The results and findings of this analysis are presented in section 2.2. The study was completed with a preliminary design and developments which are not presented here since they were rendered obsolete by the work performed in SLOTT.

2.1 State-of-the-art review of time-resolved techniques

This review focus on techniques that are potentially applicable to stray light measurement. Thus, this review discarded techniques such as triangulation, intensity-based or confocal sensing since they respectively require different viewpoints, a priori knowledge about target reflectance or high numerical aperture.

Direct time-of-flight LiDAR

Time-of-flight (TOF) measurements can be performed either indirectly by measuring the phase shift between a continuously modulated reference signal and the reflected signal (Indirect TOF – I-TOF) or directly by measuring the time taken by a short light pulse to travel back and forth to a target (Direct TOF – D-TOF) as illustrated by Figure 1. The first method suffers from an important limitation that precludes its applicability to straylight analysis: multiple echoes cannot be resolved.

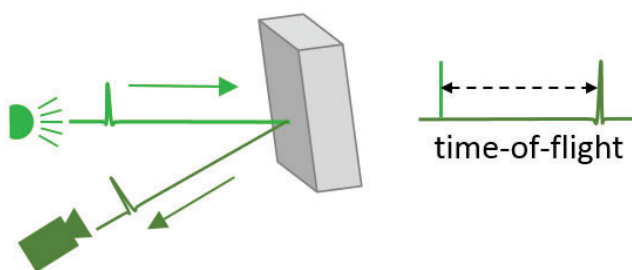


Figure 1. Principle of direct TOF measurement

Practical implementations are usually realized based on a laser source emitting short light pulses (typically in the 1-10 ns range) and a highly sensitive sensor such as an APD, a single-photon APD (SPAD) or a silicon photomultiplier (SiPM), which consists of an array of SPADs connected in parallel. SPADs are produced by operating an APD in Geiger mode, which means that a reverse-bias voltage above the breakdown voltage is applied. These detectors provide a very high sensitivity down to single-photon level but are also characterized by a certain time jitter, dark noise and dead-time (~100 ns). Dark noise can be reduced by cooling the detector and limiting the exposure to small time windows. Dead-time does

not represent an issue here because it does not affect the reliability of the measurement but simply limits the acquisition frequency and thus overall duration.

The emission of light pulses triggers the start of a time-to-digital converter (TDC) that is stopped by the output of the photodetector. The ambiguity distance is determined by the laser pulse repetition frequency (PRF). In practice, we need to ensure that a pulse has been detected before the emission of a subsequent pulse.

The distance resolution is directly affected by the TDC resolution and the SNR, whereas the precision is limited by the time jitter of the detection unit (detector, amplifier, and digitizer) and the laser pulse width. The precision is importantly enhanced by performing statistics over a certain number of measurements and identifying the reflection peak position with dedicated algorithms. This also allows the detection of multiple echoes.

Assuming statistics are performed over several measurements, the time histogram of photon counts will follow a distribution corresponding to the convolution between the laser pulse shape and the SPAD jitter distribution. Potentially, with pulse durations well below the SPAD jitter, we may achieve time resolutions in the order of 20-50 ps. Since both the detector time jitter and the laser pulse follow a distribution that can be characterised, fitting the measured histogram with this a priori knowledge can lead to improved time resolution.

Recently, a SPAD-based setup for time-resolved stray light characterization was applied for the test campaign preparation of the FLEX space telescope, allowing to discriminate stray light paths with a difference of a few millimetres and within a window of 20 meters [1].

Streak camera

The streak camera represents an interesting alternative detector for direct TOF measurements. This technology, developed by Hamamatsu, offers picosecond time resolution when employed with a small entrance slit. The principle is illustrated in Figure 2.

The signal to be analyzed passes through an entrance slit, which is then imaged onto a photocathode. This device generates photo-electrons proportionally to the light intensity. These emitted electrons are then accelerated and pass in between two electrodes that are rapidly swept with a high voltage. The generated electric field deflects electrons before their amplification by a photomultiplier, i.e. micro-channel plate (MCP). Finally, these electric charges are reconverted into light by a phosphor screen and imaged by a highly sensitive camera (not shown in Figure 2).

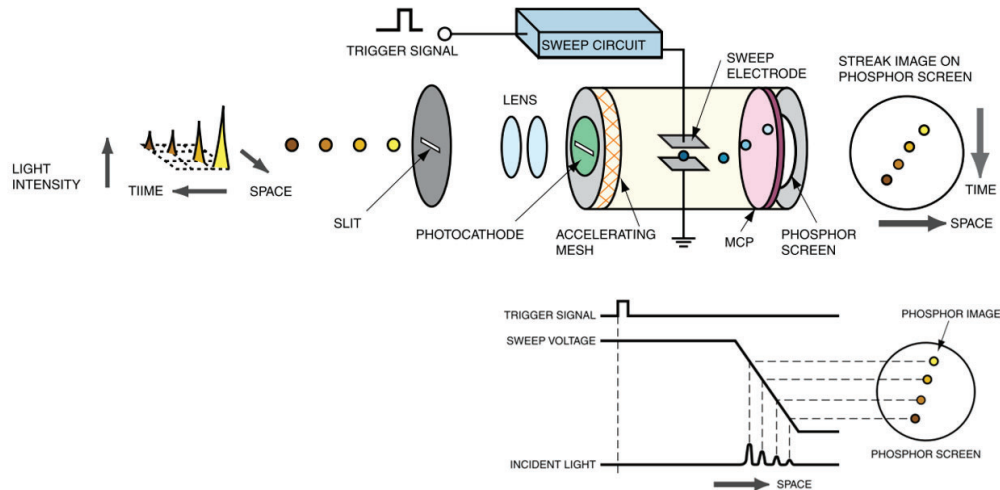


Figure 2. Operating principle and timing of the streak camera for a single sweep [2]

Thanks to very short sweep periods down to 100 ps, two light pulses separated by a few ps will be clearly separated onto the phosphor screen. Since the sweep window is relatively short (100 ps = 3 cm), a trigger and adjustable delay are necessary to scan over large ranges through multiple acquisitions. The precision is mainly limited by the timing jitter of this delay unit since cumulative measurements are usually necessary for low photon counts.

In terms of sensitivity, single photon detection has been reported when used with long integration times lasting about 15 s [3]. Taking into account the fact that each measurement represents a maximal distance of 3 cm (with a sweep period of 100 ps), a single scan along the axial dimension (no spatial scanning in x/y) would take about 25 minutes for a 3 m distance. The slit length presents a certain extent in the order of 17 mm [4] along the x-axis, the scanning time would be reduced in comparison to a single pixel detector. The time-resolved stray light measurement using a streak camera has been demonstrated in [5], characterizing ghosts and scatter paths in a refractive telescope with high spatial and temporal resolution.

Interferometry

Interferometric methods enable measuring distances down to a resolution of a few micrometres. This comes at the expense of a more complex scheme requiring important stability and a certain degree of coherence between the two arms (Michelson or Mach-Zehnder configuration). In the case of TRIPP, this represents a limitation as we expect incoherent scattering on metallic parts such as baffles. Moreover, multiple diffused reflections are known to diminish coherence [6].

Among the different methods reviewed, frequency-modulated continuous-wave (FMCW) LiDAR [7] and dual-comb interferometry [8] appear to be the most adequate, thanks to their relatively simple implementation and promising sensitivity. Concerning this latter, the detection of light levels 110 dB below the reference arm power has been reported for FMCW [9]. In theory, the ultimate sensitivity of dual-comb interferometry is situated around 120 dB [10]. Moreover, thanks to a long ambiguity range, they do not require an axial scan. Recently, Takakura et al. applied the FMCW for the Litebird space instrument for stray light characterization in the mm wavelengths [11].

Independently from the implemented interferometric technique, in order to benefit from the maximal coherent amplification and thus sensitivity, it is necessary to work in a shot-noise limited regime. This is achieved by setting the reference arm power close to the saturation level of the photodiode (typically 1-10 mW). Assuming a 1 mW saturation level and taking into account a sensitivity of 120 dB, this allows detecting power levels down to 1 fW.

Since the contrast heavily depends on the mode distributions, we could show that coupling light into single-mode fibres (SMF) is mandatory to ensure a proper contrast, which strongly affects the collection efficiency, and thus, sensitivity. This could partially be compensated by placing a lens in front of the fibre, with the drawback of having a collection efficiency very sensitive to the incidence angle onto the lens.

Recently, in the frame of the LISA space mission, low-coherence interferometry was applied to characterize and identify scattering interfaces and measure back-reflectance down to 10^{-11} levels [12].

Point-diffraction common-path interferometry

This technique allows analysing a distorted sample wavefront with respect to a filtered flat reference wavefront. Distortions of the sample beam can be manifold. Among typical defects that can be imaged, we can cite ghost images, optical surface defects and roughness, and light scattering originating from the optical system housing or dust particles.

This system can be employed in different modes and gives access to essential information to characterize systems' imaging quality. Analysis methods are dedicated to obtain PSF and overall wavefront distortions. The method's applicability to straylight analysis is indirect (e.g. wavefront filtering, dark-field) and qualitative. The application of this technique to large telescope instruments would be challenging due to the use of the double-path configuration. However, this solution is of interest as a complementary method at components or sub-systems level to assess the imaging quality of single refractive elements or blocks of a few elements.

Quantitative comparison of time-resolved techniques

Three of the different techniques presented above were compared quantitatively taking into account the performances of key COTS components selected for their implementation. Five main criteria have been selected: time resolution, sensitivity, acquisition time, rough order of magnitude (ROM) cost (i.e. laser and detector) and wavelength range.

The dynamic range was not selected since the sensitivity is sufficient to rate the different techniques. The inherent detection dynamic range is about 30 dB for the streak camera and 40 dB for SPAD and interferometry. Assuming the use of attenuators, the dynamic range of each technique can be easily extended by at least 80 dB, being sufficient for evaluating a PST over the required range. The result of the comparison is shown in Figure 5 in the form of a radar chart, where each axis is oriented in such a way that the outermost position is preferred. It is noteworthy that each axis of this radar plot is not linearly scaled.

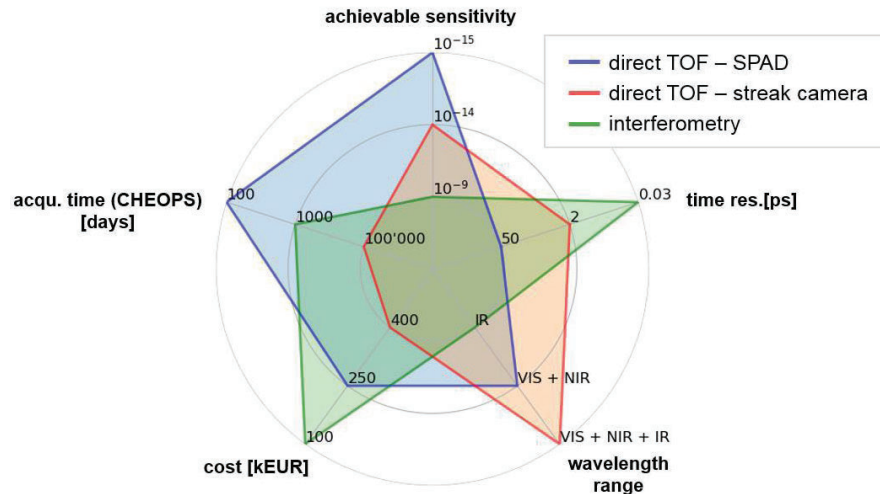


Figure 3. Quantitative comparison of three time-resolved techniques in the frame of a possible application to straylight characterization

Time resolution, sensitivity and acquisition time are defining the performance of the considered technique. Interestingly, all three techniques compare quite differently over these main criteria of interest. The SPAD-based implementation presents the most promising sensitivity and acquisition time but suffers from a limited time resolution. On the other hand, interferometry offers an unbeaten time resolution, but its sensitivity is four orders of magnitude below the requirement for CHEOPS and six orders of magnitude below the two other techniques. Moreover, one shall not neglect the fact that scanning a whole focal plane array with a single SMF slows down the acquisition time and requires a scanning mechanism. Finally, as discussed before, the streak camera requires an acquisition time not compatible with the intended application. This is essentially due to the need for an axial scanning system and the relatively small detector light collecting area.

For the wavelength range, interferometry is mainly limited to 1.5 μm due to the availability of laser sources fitting the application needs: laser sources with tuneable wavelengths are required. A SPAD-based technique would offer the best results in the visible range due to the better performances of silicon detectors in comparison to InGaAs (i.e. dark counts). The streak camera presents the advantage of being sensitive over a very large spectrum, from X-Rays to infrared.

As an outcome, despite its lower time resolution of 20-50 ps, a system based on direct TOF measurements with a detector made out of an array of SPADs combined with micro-lenses appears to be the most promising method for the following reasons:

- This technique offers sufficient sensitivity to characterize typical PST attenuations (10^{-13}).
- The acquisition time for a full instrument's characterization is compatible with foreseen requirements: a few hours at most.
- The system design offers a lot of flexibility depending on the actual needs, which allows better trade-offs in terms of sensitivity, focal plane resolution and sensitivity.

2.2 Analysis of the high-speed photon imaging application for the verification of straylight performance

To assess the potential performance of a system based on direct TOF measurements, the TRIPP project used the CHEOPS telescope as a study case. The objective of this analysis is threefold:

- Evaluate the sensitivity of the system: how much power is needed to get some straylight measurement signal.
- Evaluate the time resolution required for significant time-resolved measurements.
- Evaluate the spatial resolution required for significant imaging measurements.

To perform this analysis the consortium used the ASAP optical software.

CHEOPS geometrical model

For the TRIPP analysis, several references were available to implement the model in ASAP: a STEP file provided by ESA containing the fore and main baffles, the optical design [13], and additional information [14]. An uncertainty was remaining about the incorporation of a PSF shaping device at the time of the analysis [15], [14], [16]. Therefore, this component was omitted in the model used.

The optical model of CodeV and the CAD model were merged within ASAP. Because of the rotational symmetry the alignment of the CAD with the optical model needed to be done along only one degree of freedom: their respective longitudinal positions. This alignment was performed based on the edge ray (see Figure 4) by assuming that a ray, drawn from the edge of the entrance vane towards the edge of the third vane of the Fore Baffle, just misses the Secondary Mirror and the Primary Mirror on its later trajectory. This condition must be met, as scatter from the Fore Baffle should not hit optical surfaces directly (PM) nor objects inside the optical envelope (SM side surfaces).

The naming of different parts is given in Figure 4. The Optical Telescope Assembly is referred to as OTA, the Primary mirror as PM, the Secondary Mirror as SM and the Back End Optics as BEO.

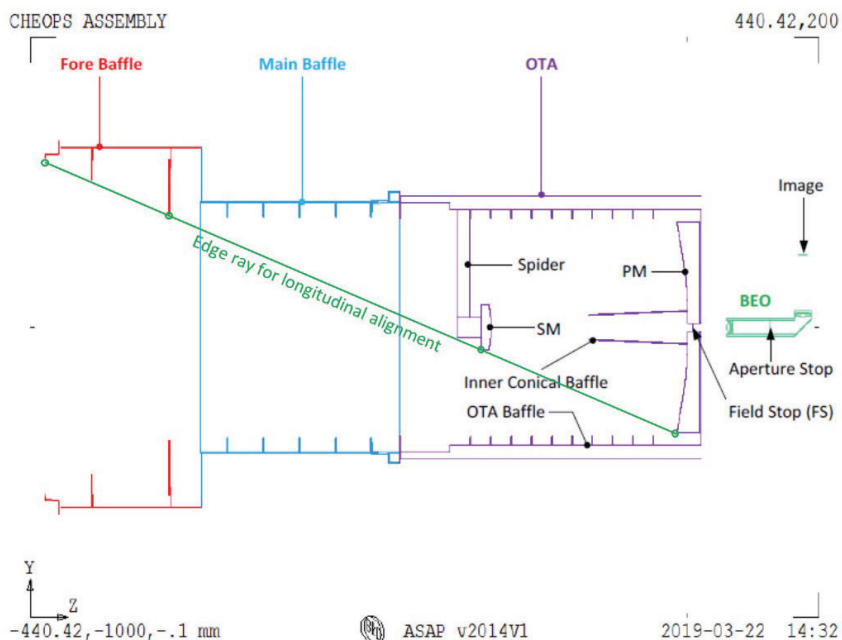


Figure 4: CHEOPS model

The next step consisted in determining critical and hot objects. Critical objects are objects that can either be directly seen by the detector or via reflections on different surfaces (eg., optical surfaces, optical and part mounts, etc.) Ghost images are also considered critical objects. Hot objects are objects which are illuminated from off-axis point sources at the limiting angle and beyond. The illumination could happen either directly or via optical surfaces. The illumination shall also account for potential ghost image paths.

The limiting angle, 35° for CHEOPS, is the specified angle beyond which the system must be shielded as far as possible from point (sun) and extended (earth, moon) straylight sources. The design of the baffle takes into account this limiting angle as the major input parameter.

Considered Bidirectional Reflectance Distribution Function (BRDF) models

The models considered the optical surfaces as mirrors with the following roughness:

- Primary mirror: roughness $R_q = 1.06$ nm
- Secondary mirror: roughness $R_q = 0.5$ nm

The other surfaces (Baffle, Vanes...) were assumed to be coated with Acktar black coating and simulated using the following parameters:

- Hemispherical Reflectance of the surface: 2%
- BRDF shape of the surface: Lambertian
- Radius of the vane tips: 0.01 mm
- Reflectance of the vane tips: 20%

Straylight analysis method

The method of the straylight analysis versus off-axis sources performed is detailed in [17] and follows the steps hereafter:

1. Determination of Critical Objects:
 - the primary mirror surface (by design),
 - the secondary mirror surface (by design),
 - the inside surface of the inner conical baffle,
 - the rear side surface of the OTA baffle,
 - the rear side surface side of the spider,
 - the side surface of the secondary mirror,
 - the front side surface of the inner conical baffle.
2. Determination of Hot Objects: In the case of CHEOPS, the limiting angle is 35° and with the design of its two-stage baffle, the only two Hot Objects identified are the Fore baffle and the Main baffle.
3. Connection of Hot Objects with Critical Objects: A case-by-case list is compiled, pairing each hot object with each critical object, one by one. The Hot Objects get scatter properties assigned with targets towards the particular Critical Objects, either directly or to their images through the PM and/or SM. The Critical Objects get scatter properties assigned with targets towards the image of the detector in the particular optical space. The result is an ASAP executable program.
4. Computation of Point source Transmittances (PST): The compiled list obtained in the previous step is executed for a series of input angles and the results are recorded. The obtained results are initially flux values found at the detector. These flux values are converted into irradiances and normalized to the input irradiance. The final PST results are computed as functions of the incidence angle θ_i at the front entrance as per equation (1). In the case of CHEOPS, with $\theta_i \geq 35^\circ$

$$\text{PST}(\theta_i) = \frac{\text{Irradiance at the detector}}{\text{Irradiance at the entrance}} \quad (1)$$

In the results presented below, the PST values are provided for $\theta_i = 35^\circ$ as this is expected to be the worst-case incidence angle.

In usual Straylight Analysis versus off-axis sources, an additional step can be performed where the PST functions are fed to a Broad Source Integration tool (Breault BSI or SALSA [18]). This BSI tool simulates a broad celestial source (i.e. Earth) for various illumination conditions (CHEOPS: day-night line in Nadir direction) and various Horizon angles with respect to the optical axis (CHEOPS: 35°) and uses the input PST to compute the integrated flux (from the Earth) reaching the detector. This last step was not performed as the TRIPP activity is limited to Point Sources (i.e. Laser).

Straylight analysis results

First, a classical straylight was performed. The corresponding results are summarized in Table 1. In this table, the results are sorted by their PST contribution. Furthermore, a normal label (example: Main baffle) indicates a scattered reflection while specular reflections are underlined (example: Primary mirror). The PST value provided is given for $\theta_i = 35^\circ$.

Table 1. Classical straylight results

Reflecting surface					PST ($\theta_i = 35^\circ$)	Number of rays
#1	#2	#3	#4	#5		
Main baffle	Primary mirror				$3.40 \cdot 10^{-11}$	166'722
Main baffle	Conical baffle	<u>Secondary mirror</u>			$2.04 \cdot 10^{-11}$	29'992
Main baffle	Conical baffle	<u>Primary mirror</u>			$9.26 \cdot 10^{-12}$	32'806
Main baffle	<u>Primary mirror</u>	Secondary mirror			$8.64 \cdot 10^{-12}$	141'892
Main baffle	OTA baffle	Spider	<u>Primary mirror</u>		$4.63 \cdot 10^{-12}$	644'226
Main baffle	OTA baffle	Primary mirror			$1.08 \cdot 10^{-13}$	1'700'944
Main baffle	<u>Primary mirror</u>	OTA baffle	Spider	<u>Primary mirror</u>	$8.95 \cdot 10^{-14}$	711'818
Main baffle	OTA baffle	Secondary mirror			$7.60 \cdot 10^{-14}$	2'239'154
Fore baffle	Main baffle	Primary mirror			$4.94 \cdot 10^{-14}$	146'975
Main baffle	OTA baffle	<u>Primary mirror</u>	Spider	<u>Primary mirror</u>	$3.70 \cdot 10^{-14}$	584'455
Main baffle	<u>Multiple</u> ¹	OTA baffle	Spider	<u>Primary mirror</u>	$1.23 \cdot 10^{-14}$	541'829
Main baffle	<u>Multiple</u> ²	OTA baffle	Spider	<u>Primary mirror</u>	$2.19 \cdot 10^{-16}$	20'287
Fore baffle	OTA baffle	Primary mirror			$5.86 \cdot 10^{-17}$	7'212
Fore baffle	Main baffle	<u>Primary mirror</u>	Secondary mirror		$3.09 \cdot 10^{-17}$	4'404
Total					$7.73 \cdot 10^{-11}$	6'972'716

¹ Multiple specular reflections: → Primary mirror → Secondary mirror →

² Multiple specular reflections: → Primary mirror → Secondary mirror → Primary mirror →

Then temporal profiles were simulated for a range of optical path lengths (OPL) between 1.2 meters and 4.8 meters, thus a temporal range of up to 16 ns. The found OPL spanned between 1.7 meters (5.67 ns) and 3.6 meters (12 ns). The major contribution is found in the range between 5.7 ns (1.7 m) and 6.7 ns (2 m). Each contribution was simulated individually, leading to an entire analysis of the system.

Timeline profiles were computed for three different time resolutions. Sums of all contributions are depicted in Figure 5, Figure 6, and Figure 7 for the respective time resolution of 50 ps (15 mm), 12 ps (3.6 mm) and 1 ps (0.3 mm).

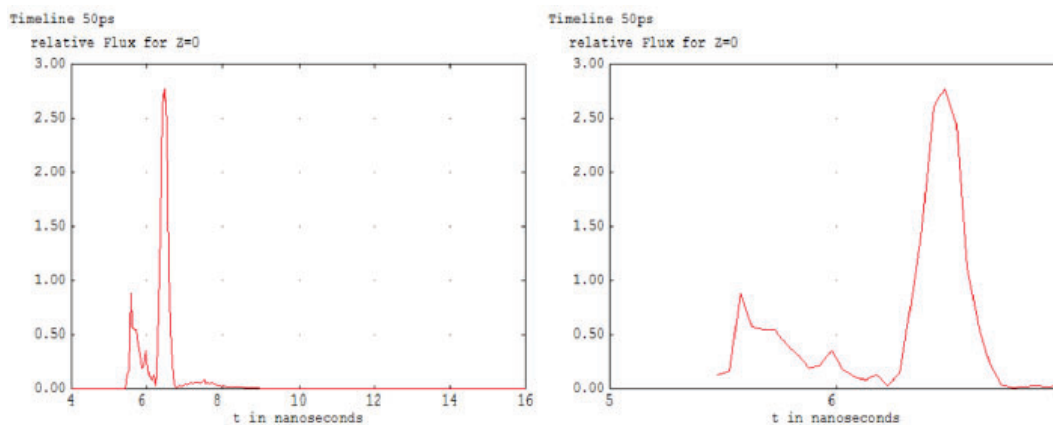


Figure 5. Simulated timeline profile with 50 ps time resolution (left: full temporal range; right: zoom between 5 ns and 7 ns)

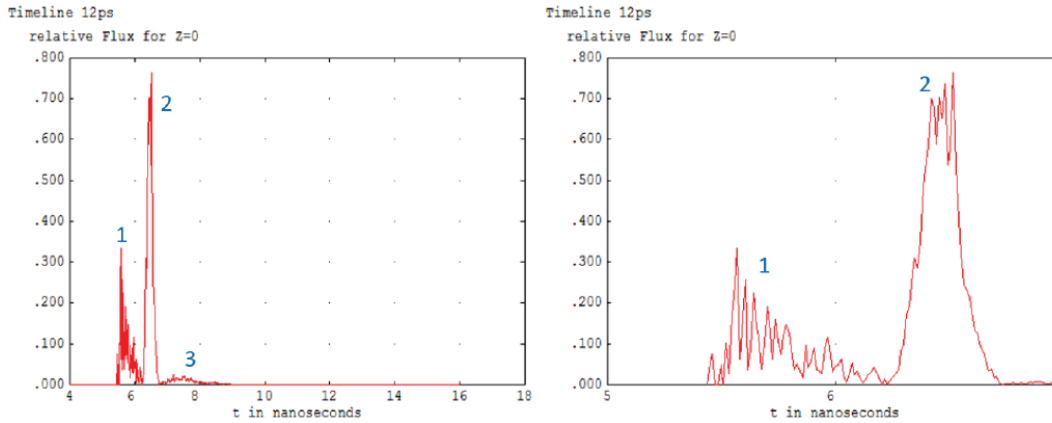


Figure 6. Simulated timeline profile with 12 ps time resolution (left: full temporal range; right: zoom between 5 ns and 7 ns)

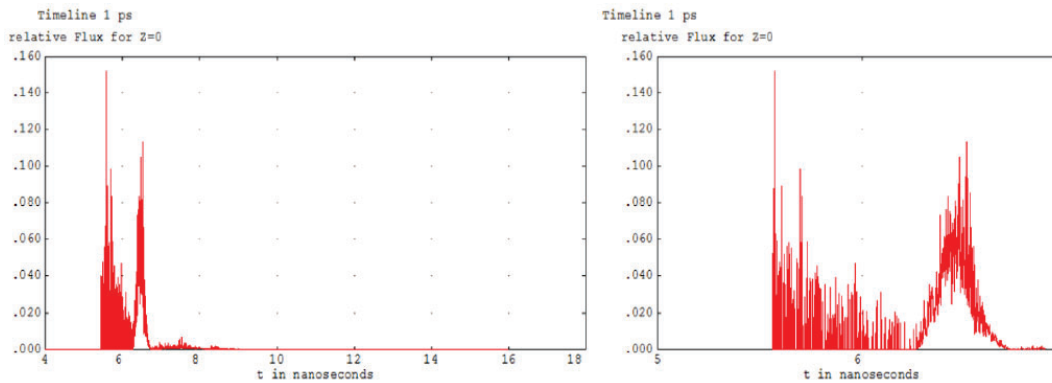


Figure 7. Simulated timeline profile with 1 ps time resolution (left: full temporal range; right: zoom between 5 ns and 7 ns)

In the above figures, three main regions can be identified, numbered from 1 to 3 in Figure 6. These regions correspond to the following straylight contributions:

1. Scatter at Main Baffle → Scatter Inner Conical Baffle → Reflection to SM → Image
2. Three contributions:
 - a. Scatter at Main Baffle → Scatter at PM → Image
 - b. Scatter at Main Baffle → Scatter at Inner Conical Baffle → Reflection at PM → Image
 - c. Scatter at Main Baffle → Reflection at PM → Scatter at SM → Image
3. Various paths with the involvement of the Spider

The second region contains three contributors, which can hardly be distinguished. A resolution of 50 ps is not sufficient to distinguish the different peaks, whereas a resolution of 12 ps allows their differentiation. In simulations, an enhanced time resolution of 1 ps as illustrated by Figure 7, does not permit the identification either, partially due to numerical noise.

Finally, a spatial resolution of 160x160 pixels distributed over the whole CHEOPS detector (~80 μm/pixel) was simulated. The aim of this latter analysis consisted in verifying whether relying on the spatial resolution would provide meaningful information. The resulting spatial distribution for all straylight contributions is shown in Figure 8, together with two single important contributions.

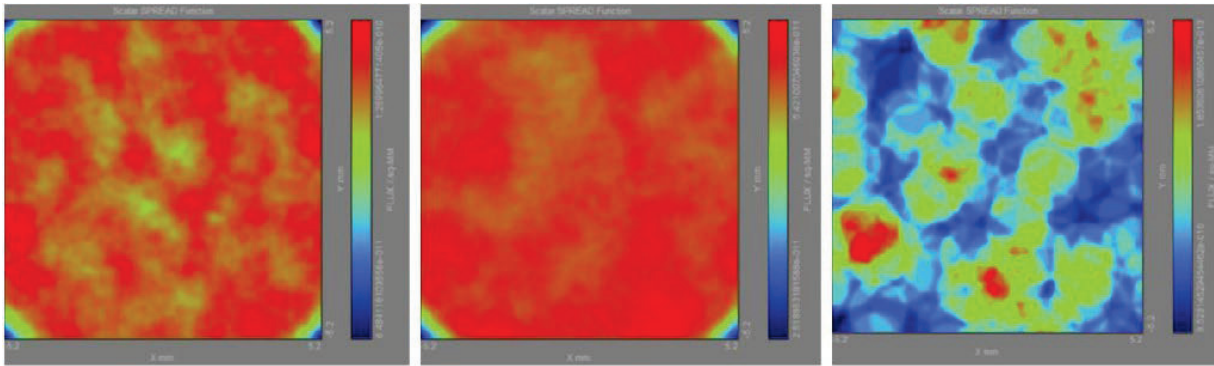


Figure 8. Simulated spatial distribution of straylight (left: for the sum of all contributions; centre: for the contribution “Main baffle → Primary mirror → Image”; right: for the contribution “Fore baffle → Main baffle → Primary mirror → Image”)

As it can be seen in Figure 8, identifying straylight contributions based on their spatial distribution appears to be very challenging, and even impossible for certain contributions: the patterns generated by each contribution are blended together and do not seem to follow any specific geometry which would render them identifiable in the obtained sum of contribution.

Conclusion of the analysis

Overall, the analysis results proved to be insightful and in line with previous simulations of CHEOPS presented so far in the literature [13], [15]. This work also shows that:

1. A time resolution in the order of 10 ps shall be the aim for a future instrument to give valuable insights on straylight performances. However, 20 to 30 ps could also be an acceptable minimum, especially for the chosen test case of CHEOPS.
2. **Straylight contributions are not localized in particular positions of the focal plane but spread rather homogeneously over the detector. Resolving straylight paths spatially is thus not an option and the TRIPP instrument shall mostly rely on time resolution to discriminate different straylight contributions from one another.** This relaxes the requirement in terms of detector spatial resolution but emphasizes the need for time resolution.

This is a key finding, which was not anticipated, and fundamentally changes the approach from a combination of image resolved timing, to predominantly precision timing.

3. A trade-off between sensitivity and acquisition time may be mandatory depending on the payload under test. Special care shall be taken to devise the scanning scheme to limit the acquisition time. For example, the scanning of the TRIPP instrument shall enable, either a complete raster scan of the payload or, a focus on the most significant paths that have been identified in the high fidelity simulations already carried out.

3. SLOTT – THE DESIGN OF A BREADBOARD STRAYLIGHT LIDAR OGSE

3.1 Objectives of the SLOTT development

Capitalizing on the outcomes of the TRIPP study, the SLOTT development started in June 2021 to demonstrate through the test the possibility to acquire time-resolved straylight information which would help discriminate between the various straylight contributors. Toward this main objective, a demonstrator straylight measurement OGSE tool thereafter referred to as SLOTT Breadboard, will be developed and tested onto the CHEOPS baffle (the assembly comprising the Fore and Main Baffle). The main requirements targeted by the activity are listed in Table 2.

Table 2. SLOTT breadboard main requirements

Requirement	Targeted value	Expected compliance
Range resolution / timing resolution	$\leq 10 \text{ mm} / \leq 33 \text{ ps}$	Yes
Minimal detectable Point source transmittance	$\leq 10^{-13}$	Yes
Operational wavelengths	From 400nm to 1700nm	No (see Table 3)
Telescope entrance aperture	Up to 1 m	Yes, depending on the angle of incidence
Illuminator scanning spatial resolution	$\leq 10 \text{ mm}$	Yes
Range of Angle of incidence	Elevation from 0° to 90° Azimuth from 0° to 180°	No (see Table 3)
Resolution of Angle of incidence	Elevation better than 0.1° Azimuth better than 1°	Yes

3.2 Overview of the design

To fulfil its purpose, the SLOTT breadboard emits laser light pulses into the tested item and measures the outgoing light intensity and time of flight. Thus, it is composed of:

- An illumination module, equipped with a Femtosecond Laser and a scanning mechanism.
- A detection and timing system, equipped with a Single-photon detector and associated time of flight measurement electronics.
- A control computer to operate the various subsystems.

The tested item is placed between the illumination module and the detector system. The overall design of the SLOTT breadboard is illustrated in Figure 9 and Figure 10.

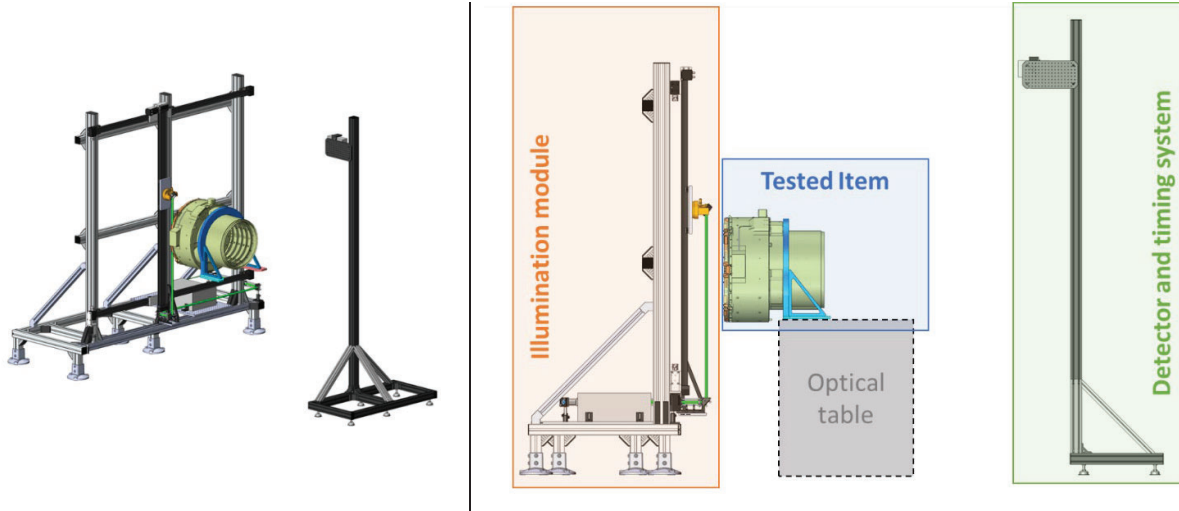


Figure 9. SLOTT breadboard overall CAD implementation – electronics systems such as the control computer, TCSPC and delay box are not illustrated here but will be implemented on the base of the detector and timing system (left: isometric view; right: side view)

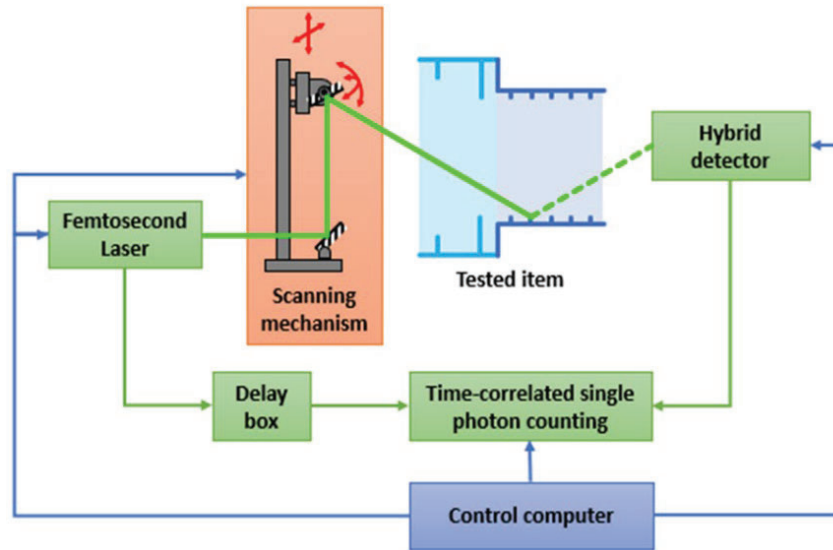


Figure 10. SLOTT breadboard overall architecture

The main parameters expected of this design are collected and presented in Table 3.

Table 3. Main parameters of the SLOTT Breadboard

	Parameters	Value
Laser parameters	Wavelength	520 nm
	Laser average power	3 W
	Repetition rate	40 MHz
	Laser pulse energy	75 nJ
	Illumination beam diameter ¹	Adaptable: 2, 6.7, 10, 16.7 and 26.6 mm
Detection and timing system parameters	Expected time resolution	< 20 ps (correspond to ~ 6 mm)
	Quantum efficiency (@520 nm)	10 %
	Active area	Ø 3 mm (7.06 mm ²)
	Dark count	50 cps
Scanning mechanism parameters	X-axis translation range (horizontal)	1 500 mm
	Y-axis translation range (vertical)	1 250 mm
	Translation repeatability (X and Y)	0.5 mm
	Øx-axis gimbal range	0° to -65° (manual gimbal)
	Øy-axis gimbal range	-65° to +65° (manual gimbal)

¹ The beam waist can be configured to be down to 2 mm when no beam expander is implemented. However, this is not recommended as the collimation of such a narrow beam is not sufficient for the range of operation of the laser. At a minimum, a beam waist of 6.7 mm is needed.

3.3 The time-of-flight measurement chain

The time of flight measurement chain is composed of:

- A femtosecond laser from [Prospective Instruments](#)² to emits light pulses
- A hybrid detector, to detect light pulses scattered and reflected by the tested item
- A Time-correlated single photon counting (TCSPC) system from [Becker & Hickl](#)³, to measure the time between the emission and the detection of the light pulses
- A delay box, to delay the laser synchronous pulses: this allows the operation of the TCSPC in reversed start-stop mode which enables fast acquisition of successful pulses (at repetition rates up to 100 MHz)[19].

The operation of the time-of-flight measurement chain can be resumed as below:

The femtosecond laser is fired, generating simultaneously a light pulse toward the tested item and a synchronized electronic pulse toward the TCSPC. The light pulse is then scattered and reflected multiple times inside the tested item. Part of the light pulse is finally collected by the detector which then generates a pulse toward the TCSPC. Meanwhile, the laser synchronized electronic pulse is delayed by the delay box. The TCSPC measure the time between the detector pulse, which is received first and the delayed synchronized electronic pulse. As the delay time is a known value, the time between the emission and the reception of the light pulse can be known. Such sequence is repeated many times for every measurement point to collect some statistics about the time distribution of detected photons.

3.4 Known limitations of the SLOTT breadboard and activity

While the SLOTT breadboard design can fully address the objective of the activity, it was greatly constrained by the overall budget allocated to the development. The objective of the activity is to demonstrate the possibility of performing time-resolved straylight measurements. Thus, the budget was defined accordingly with the knowledge that another development step would be required to get a fully functional time-resolved straylight tool achieving the desired performances. The current main limitations of the design are:

- The laser source selection is constrained by the cost budget. A fruitful collaboration with [Prospective Instruments](#)² gave access to a very well-suited laser fitting the project price range. However, more powerful sources can be found and would be useful in future developments to extend the range of measurable PST.
- The illumination scanning mechanism is equipped with a manual gimbal. For demonstration purposes, such a solution is acceptable even if it increases the measurement time and thus limits the number of field angles tested during the demonstration. In the final time-resolved straylight tool, a motorized gimbal will be necessary to enable a complete scanning of the telescope's field of view.
- The current SLOTT breadboard design is tuned to the test of the CHEOPS baffle, thus placing the detector at convenient locations which are not representative of any telescope test configuration. In the future, the detector would be placed in the focal plane of the telescope. Additionally, a detector scanning mechanism may be implemented to perform scans of the complete telescope detector area.
- The current design of the SLOTT breadboard is using a single 520 nm Laser. Measurements are thus limited to that wavelength. However, the detector used is sensitive from 220 nm to 850 nm and other sensors can be envisaged to extend slightly this spectral range toward the NIR infrared. Such sensors were not selected here because of their poorer timing performance. However, to acquire measurements in the IR spectrum (above 1000 nm), the silicon-based detector cannot be used anymore. Current InGaAs detectors are not compatible with the application's needs for ultra-fast response time. A solution may be found with superconducting NbN detectors but needs to be further investigated as such a system was well out of the scope of the SLOTT development.

Even if the SLOTT breadboard does not implement any of these features, the design is already adapted to allow future upgrades of the system toward a fully functional time-resolved straylight measurement tool.

² More information at: <https://www.p-inst.com/>

³ More information at: <https://www.becker-hickl.com/>

4. CONCLUSION

Through the TRIPP study and the ongoing SLOTT activity, CSEM and its partners are developing a promising straylight measurement tool. We expect that the upcoming tests will clearly demonstrate the potential of such techniques, hopefully establishing new methods to characterize and reduce the straylight propagation in future space-based telescopes. Such results are expected toward the end of the SLOTT activity planned in January 2024.

REFERENCES

- [1] L. Clermont, W. Uhring, M. Georges, W. Khaddour, P. Blain, and E. Mazy, ‘A new paradigm in the field of stray light control and characterization enabled by ultrafast time-of-flight imaging’, presented at the SPIE Astronomical telescopes + Instrumentation, Montréal, Canada, 2022. [Online]. Available: <https://spie.org/astronomical-telescopes-instrumentation/presentation/A-new-paradigm-in-the-field-of-stray-light-control/12188-48>
- [2] Hamamatsu, ‘Guide to Streak Cameras’. Hamamatsu, 2008. Accessed: Aug. 04, 2022. [Online]. Available: https://www.hamamatsu.com/content/dam/hamamatsu-photonics/sites/documents/99_SALES_LIBRARY/sys/SHSS0006E_STREAK.pdf
- [3] S. Kobayashi, M. Yamashita, T. Sato, and S. Muramatsu, ‘A single-photon sensitive synchroscan streak camera for room temperature picosecond emission dynamics of adenine and polyadenylic acid’, *IEEE J. Quantum Electron.*, vol. 20, no. 12, pp. 1383–1385, Dec. 1984, doi: 10.1109/JQE.1984.1072335.
- [4] L. Gao, J. Liang, C. Li, and L. V. Wang, ‘Single-shot compressed ultrafast photography at one hundred billion frames per second’, *Nature*, vol. 516, no. 7529, Art. no. 7529, Dec. 2014, doi: 10.1038/nature14005.
- [5] L. Clermont, W. Uhring, and M. Georges, ‘Stray light characterization with ultrafast time-of-flight imaging’, *Sci. Rep.*, vol. 11, no. 1, p. 10081, Dec. 2021, doi: 10.1038/s41598-021-89324-y.
- [6] A. Velten, T. Willwacher, O. Gupta, A. Veeraraghavan, M. G. Bawendi, and R. Raskar, ‘Recovering three-dimensional shape around a corner using ultrafast time-of-flight imaging’, *Nat. Commun.*, vol. 3, no. 1, Art. no. 1, Mar. 2012, doi: 10.1038/ncomms1747.
- [7] M.-C. Amann, T. M. Bosch, M. Lescure, R. A. Myllylae, and M. Rioux, ‘Laser ranging: a critical review of unusual techniques for distance measurement’, *Opt. Eng.*, vol. 40, no. 1, pp. 10–19, Jan. 2001, doi: 10.1117/1.1330700.
- [8] I. Coddington, W. C. Swann, L. Nenadovic, and N. R. Newbury, ‘Rapid and precise absolute distance measurements at long range’, *Nat. Photonics*, vol. 3, no. 6, Art. no. 6, Jun. 2009, doi: 10.1038/nphoton.2009.94.
- [9] E. Baumann, F. R. Giorgetta, J.-D. Deschênes, W. C. Swann, I. Coddington, and N. R. Newbury, ‘Comb-calibrated laser ranging for three-dimensional surface profiling with micrometer-level precision at a distance’, *Opt. Express*, vol. 22, no. 21, pp. 24914–24928, Oct. 2014, doi: 10.1364/OE.22.024914.
- [10] I. Coddington, N. Newbury, and W. Swann, ‘Dual-comb spectroscopy’, *Optica*, vol. 3, no. 4, pp. 414–426, Apr. 2016, doi: 10.1364/OPTICA.3.000414.
- [11] H. Takakura *et al.*, ‘Straylight identification of a crossed-Dragone telescope by time-gated near-field antenna pattern measurements’, presented at the SPIE Astronomical telescopes + Instrumentation, Montréal, Canada, 2022. [Online]. Available: <https://spie.org/astronomical-telescopes-instrumentation/presentation/Stray-light-identification-of-the-LiteBIRD-Low-Frequency-Telescope-scaled/12180-231>
- [12] I. Khan, M. Lequime, M. Zerrad, and C. Amra, ‘Detection of Ultralow Light Power Back-Reflected or Back-Scattered by Optical Components Using Balanced Low-Coherence Interferometry’, *Phys. Rev. Appl.*, vol. 16, no. 4, p. 044055, Oct. 2021, doi: 10.1103/PhysRevApplied.16.044055.
- [13] ESA, ‘CHEOPS Definition Study Report’, Definition Study Report ESA/SRE(2013)7, Nov. 2013. Accessed: Aug. 04, 2022. [Online]. Available: https://sci.esa.int/documents/34375/36249/1567259940843-CHEOPS_EST_SCI_RP_001_RedBook_i1.0.pdf
- [14] D. Magrin *et al.*, ‘Shaping the PSF to nearly top-hat profile: CHEOPS laboratory results’, Aug. 2014, vol. 9143, p. 91434L. doi: 10.1117/12.2055858.
- [15] T. Beck *et al.*, ‘CHEOPS: status summary of the instrument development’, Edinburgh, United Kingdom, Jul. 2016, p. 99042A. doi: 10.1117/12.2234562.
- [16] A. Fortier *et al.*, ‘CHEOPS: a space telescope for ultra-high precision photometry of exoplanet transits’, in *Space Telescopes and Instrumentation 2014: Optical, Infrared, and Millimeter Wave*, Aug. 2014, vol. 9143, pp. 750–761. doi: 10.1117/12.2056687.
- [17] E. C. Fest, *Stray light analysis and control*. Bellingham, Washington: SPIE Press, 2013.

- [18] T. Kuntzer, A. Fortier, and W. Benz, 'SALSA: a tool to estimate the stray light contamination for low-Earth orbit observatories', in *Observatory Operations: Strategies, Processes, and Systems V*, Aug. 2014, vol. 9149, pp. 347–356. doi: 10.1117/12.2055829.
- [19] W. Becker, 'The bh TCSPC Handbook', 9th edition, 2021. Accessed: Aug. 10, 2022. [Online]. Available: <https://www.becker-hickl.com/literature/documents/flim/the-bh-tcspc-handbook/>